Heiligers, J., Ceriotti, M., McInnes, C.R., and Biggs, J.D. (2011) Design of optimal Earth pole-sitter transfers using low-thrust propulsion. In: 62nd International Astronautical Congress, 3-7 Oct 2011, Cape Town, South Africa.

<u>(PREPRINT) IAC-11-C1.1.11</u>

DESIGN OF OPTIMAL EARTH POLE-SITTER TRANSFERS USING LOW-THRUST PROPULSION

Jeannette Heiligers
Advanced Space Concepts Laboratory, University of Strathclyde, Glasgow, United Kingdom,
jeannette.heiligers@strath.ac.uk

Matteo Ceriotti
Advanced Space Concepts Laboratory, University of Strathclyde, Glasgow, United Kingdom,
matteo.ceriotti@strath.ac.uk

Colin R. McInnes
Advanced Space Concepts Laboratory, University of Strathclyde, Glasgow, United Kingdom,
colin.mcinnes@strath.ac.uk

James D. Biggs
Advanced Space Concepts Laboratory, University of Strathclyde, Glasgow, United Kingdom,
james.biggs@strath.ac.uk

Recent studies have shown the feasibility of an Earth pole-sitter mission using low-thrust propulsion. This mission concept involves a spacecraft following the Earth's polar axis to have a continuous, hemispherical view of one of the Earth's poles. Such a view will enhance future Earth observation and telecommunications for high latitude and polar regions. To assess the accessibility of the pole-sitter orbit, this paper investigates optimum Earth pole-sitter transfers employing low-thrust propulsion. A launch from low Earth orbit (LEO) by a Soyuz Fregat upper stage is assumed after which a solar-electric-propulsion thruster transfers the spacecraft to the pole-sitter orbit. The objective is to minimise the mass in LEO for a given spacecraft mass to be inserted into the pole-sitter orbit. The results are compared with a ballistic transfer that exploits the manifolds winding off the pole-sitter orbit. It is shown that, with respect to the ballistic case, low-thrust propulsion can achieve significant mass savings in excess of 200 kg for a pole-sitter spacecraft of 1000 kg upon insertion. To finally obtain a full low-thrust transfer from LEO up to the pole-sitter orbit, the Fregat launch is replaced by a low-thrust, minimum time spiral through an orbital averaging technique, which provides further mass savings, but at the cost of an increased time of flight.

I. INTRODUCTION

Observation of the polar regions is currently performed using data retrieved from satellites in highly inclined, low Earth orbits, restricting them to observe only narrow swaths of the polar regions during each passage. Therefore, to obtain a full view, images of different passages have to be patched together to form so-called composite images, which have poor temporal resolution. Much better temporal resolution can nowadays be obtained from geostationary (GEO) satellites, but it is well known that high latitude regions are out of sight for GEO spacecraft. Recent studies are therefore investigating alternative concepts such as extended Molniya orbits[1] and a pole-sitter platform[2]. The latter remains at a fixed position above either the North or South pole and can as such be seen as an analogue to the GEO for polar observations[3]: a pole-sitter mission would allow for a full, real time hemispherical view of the polar regions. According to Lazzara et al.[3], this would significantly enhance polar

environmental remote sensing for meteorological forecasting, to identify and track storm systems and to generate atmospheric motion vectors for which a gap exists between data from polar orbiting satellites and satellites in GEO. Furthermore, the pole-sitter could contribute to space weather monitoring. For this, auroral conditions need to be monitored continuously, because they can change rapidly and as such have major impact on radar operations and communications. Finally, with geostationary spacecraft out of sight in polar regions, the pole-sitter could establish critical communication links.

To maintain such a pole-sitter position, continuous low-thrust propulsion would be required to counterbalance the gravitational attraction of the Earth. The pole-sitter therefore falls in the category of non-Keplerian orbits (NKOs). The existence, stability and control of NKOs have been studied for both the two- and three body problem[4-5] and a wide range of applications has been proposed. In the two-body

problem applications include spacecraft proximity operations[6] and displaced geostationary orbits[7], while three-body applications include NKOs in the Earth-Moon system for lunar far-side communication[8] and lunar south pole coverage[9].

The application of NKOs in the form of the pole-sitter mission was first proposed by Driver[2] and later by Forward[10], but an extensive investigation of optimal pole-sitter orbits and their control has only recently been performed by Ceriotti et al.[11]. The work considers both constant and variable altitude pole-sitters. The latter allows the Earth-spacecraft distance to be varied during the year and are optimised for the propellant consumption. For instance, for the use of solar electric propulsion (SEP) it was shown that a five year pole-sitter mission with a 100 kg payload is feasible and requires an initial mass of 465 kg. Additionally, a feedback control system has been designed to show that the orbit is controllable under unexpected conditions such as injection errors and temporary SEP failure.

Although the in-orbit phase of the pole-sitter mission has been studied in detail, the transfer from Earth to access the pole-sitter orbit is largely unexplored. Only Golan et al.[12] investigated locally optimal transfers from a circular low Earth orbit (LEO) to a so-called pole squatter, which is a highly elliptic orbit (with apogee in the order of 100 Earth radii) and therefore not a true pole-sitter. This paper therefore provides a new approach to investigate optimum, low-thrust Earth pole-sitter transfers using SEP.

The challenge that immediately arises when designing such a transfer is the fact that, to reach the pole-sitter position from LEO, the spacecraft has to increase its orbit radius by a factor 200. The result will be a long duration spiral trajectory with hundreds or even thousands of orbital revolutions and transfer times in the order of months to years[13]. When using a direct method for the trajectory optimisation this poses a severe challenge as the optimal control problem becomes complex. To deal with this issue, the pole-sitter transfer is modelled by distinguishing between a launch phase and a transfer phase. Moreover, the launch phase is initially designed as a two-body Soyuz Fregat upper stage transfer from a fixed inclination, low Earth parking orbit up to insertion into the transfer phase. The transfer phase is modelled in the Earth-Sun three-body problem, adding acceleration terms for the low-thrust propulsion system. To find optimum transfers, the objective is to minimise the mass in the low Earth parking orbit for a given spacecraft mass to be inserted into the pole-sitter orbit, thereby minimising launch mass and thus launch and mission cost. The optimisation is carried out using a direct pseudo-spectral method that solves the optimal control problem in the transfer phase and links the transfer and launch phases in the objective function. To assess the performance of

the SEP transfer and to provide an initial guess for its optimisation, also ballistic transfers that exploit the manifolds that wind onto the pole-sitter orbit will be considered.

Once the optimum transfer phase has been designed, the Fregat launch phase is replaced by a low-thrust, minimum time spiral trajectory to obtain a full low-thrust Earth to pole-sitter transfer, thereby reducing the spacecraft mass in LEO at the cost of an increased transfer time. To model the multi-revolution, long duration spiral, an orbital averaging technique, similar to that suggested by Gao[14] is employed, which includes locally optimal control laws to increase the semi-major axis, eccentricity and inclination. The optimal control problem in the spiral is subsequently solved using the same direct pseudo-spectral method as used for optimising the transfer phase.

The structure of the paper is as follows. First, a detailed definition of the pole-sitter orbit and the reference frame in which it is defined will be provided. Subsequently, the models used for the Fregat launch phase and the transfer phase will be outlined. Intermediate results for both ballistic and low-thrust transfers and transfers to both constant and variable altitude orbits will be provided and compared. Finally, the approach to replace the Fregat launch phase by a low-thrust spiral is outlined and the final results and conclusions will be given.

II. POLE-SITTER ORBIT

The pole-sitter orbit is defined in the Earth-Sun circular restricted three body problem (CR3BP). In the CR3BP the motion of an infinitely small mass, m (the pole-sitter spacecraft), is described under the influence of the gravitational attraction of two much larger masses, m_1 (Sun) and m_2 (Earth). The gravitational influence of the small mass on the larger masses is neglected and the larger masses are assumed to move in circular orbits about their centre of mass.

Fig. 1 shows the reference frame that is employed. The origin coincides with the centre of mass of the system, the x axis connects the larger masses and points in the direction of the smaller of the two, m_2, and the z axis is directed perpendicular to the plane in which the two larger masses move. The y axis completes the right handed reference frame. Finally, the frame rotates at constant angular velocity, ω, about the z axis, $\boldsymbol{\omega} = \omega\hat{\mathbf{z}}$. Furthermore, new units are introduced. The sum of the two larger masses is taken as the unit of mass, i.e. $m_1 + m_2 = 1$. Then, with the mass ratio $\mu = m_2/(m_1 + m_2)$, the masses of the large bodies become $m_1 = 1 - \mu$ and $m_2 = \mu$ (with $\mu = 0.30404 \cdot 10^{-5}$ for the Earth-Sun system). As unit of

length the distance between the main bodies is selected and $1/\omega$ is chosen as unit of time, causing $\omega = 1$.

Using this reference system, the motion of the pole-sitter spacecraft is described by:

$$\ddot{\mathbf{r}} + 2\boldsymbol{\omega} \times \dot{\mathbf{r}} = -\nabla U + \mathbf{a} \qquad [1]$$

with $\mathbf{r} = \begin{bmatrix} x & y & z \end{bmatrix}^T$ the position vector and U the effective potential that combines the gravitational potential of the central body and a potential that represents the centripetal acceleration, $U = -(1-\mu)/r_1 - \mu/r_2 - (x^2 + y^2)/2$ with $\mathbf{r}_1 = \begin{bmatrix} x+\mu & y & z \end{bmatrix}^T$ and $\mathbf{r}_2 = \begin{bmatrix} x-(1-\mu) & y & z \end{bmatrix}^T$. Finally, $\mathbf{a}$ represents a thrust-induced acceleration.

Due to the obliquity of the ecliptic and the rotation of the reference frame, the apparent motion of the Earth's polar axis describes a cone as depicted in Fig. 1. The pole-sitter spacecraft needs to track this motion of the polar axis by applying the aforementioned thrust-induced acceleration. The position, $\mathbf{r}$, and velocity, $\dot{\mathbf{r}}$, of the spacecraft at any time, t, during the year are therefore defined by:

$$\mathbf{r} = \begin{bmatrix} d \sin i_{obl} \cos\theta + (1-\mu) \\ -d \sin i_{obl} \sin\theta \\ d \cos i_{obl} \end{bmatrix} \qquad [2]$$

$$\dot{\mathbf{r}} = \begin{bmatrix} -d \sin i_{obl} \sin\theta \\ -d \sin i_{obl} \cos\theta \\ 0 \end{bmatrix} \qquad [3]$$

with $i_{obl} = 23.5°$ the obliquity of the ecliptic and $\theta = \omega t$ the instantaneous angular position of the spacecraft along the pole-sitter orbit with $\theta = 0$ at winter solstice and $\theta = \pi$ at summer solstice. Note that Fig. 1 and Eqs. [2] and [3] only consider pole-sitter orbits where the spacecraft remains at a constant distance, d, from the Earth (hence the zero velocity in z direction). However, also variable altitude pole-sitter orbits that are more fuel optimal than constant altitude pole-sitters will be considered, where the spacecraft-Earth distance is allowed to vary during the year according to the following sinusoidal law[11]:

$$d(\theta) = d_0 + (d_1 - d_0)\frac{1 - \cos\theta}{2} \qquad [4]$$

with d_0 and d_1 the distance from the Earth at winter and summer solstices, respectively, see Fig. 2. The position vector of the spacecraft in the variable altitude orbit, $\mathbf{r}_I$, is still equal to Eq. [2], but the velocity vector needs to be augmented as:

$$\dot{\mathbf{r}}_I = \dot{\mathbf{r}} + \frac{1}{2}(d_1 - d_0)\sin\theta \begin{bmatrix} \sin i_{obl} \cos\theta \\ -\sin i_{obl} \sin\theta \\ \cos i_{obl} \end{bmatrix} \qquad [5]$$

In accordance with the work in Ref. 11, this paper will consider $d = 0.01$ AU for the constant altitude pole-sitter and $d_0 = 0.01$ AU and $d_1 = 0.018$ AU for the variable altitude pole-sitter. Finally, for all cases the spacecraft mass at the start of the pole-sitter mission (that coincides with the end of the transfer phase) is assumed to be 1000 kg.
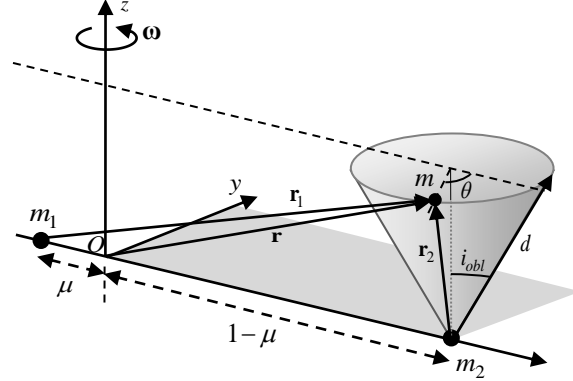

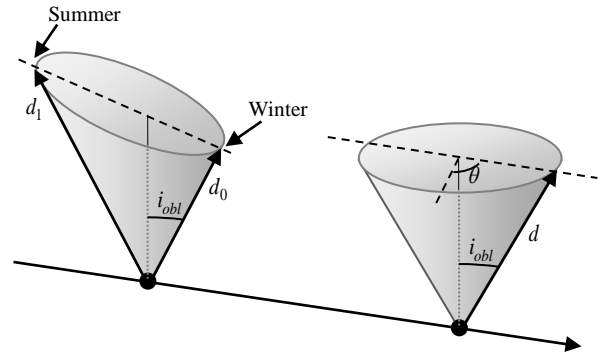Fig. 1 Schematic of pole-sitter orbit and reference frame.

Fig. 2 Schematic of constant and variable altitude pole-sitter orbits.

III. TRAJECTORY PHASES

The trajectory from LEO up to insertion into the pole-sitter orbit is modelled by distinguishing between two phases: a launch phase and a transfer phase, see Fig. 3. Note that, for now, the launch phase is assumed to be performed by a Soyuz Fregat upper stage, but will later be replaced by a low-thrust spiral in Section V. The two phases are linked by requiring that the Fregat launches the spacecraft into a two-body Keplerian orbit (marking the end of the launch phase) that coincides with the initial state vector of the transfer phase (marking the start of the transfer phase). In this section the models adopted to describe both phases will be discussed.
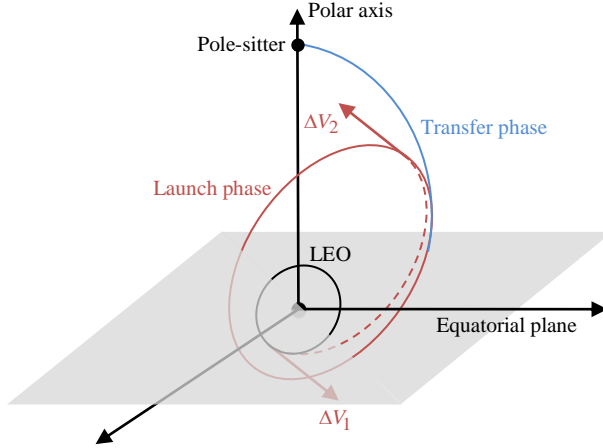
Fig. 3 Schematic of launch and transfer phases.

III.I   Launch phase

Before providing the model used to describe the launch phase, it is noted that the objective is not to provide a detailed and optimal launch strategy, but a simple, though reliable, method to assess the relative efficiency of different transfer trajectories. This implies that only non-escape launches are considered, i.e. the eccentricity upon insertion into the transfer phase is less than 1.

To model the launch phase, Ref. 15 is used which provides the Soyuz/ST launch vehicle performance through a set of reference missions, assuming a launch from Baikonur (45.6°N, 63.3°E). Due to ground-path safety rules and authorized drop-zone locations for expended stages, the first three stages can be launched into four launch azimuths, resulting into four initial parking orbit planes, see Table 1. Any remaining inclination changes can be provided by the Fregat upper stage.

Launch azimuth, deg	Reference orbit inclination, deg
60.7	51.8
34.8	64.9
25.9	70.4
-10.9	95.4

Table 1 Authorized launch azimuths and corresponding reference orbit inclinations for a Soyuz launch from Baikonur[15].

A typical non-escape Soyuz launch flight profile is provided by Ref. 15 and can be divided into the following phases. First, the three lower stages and the Fregat upper stage are used to reach a low Earth parking orbit with an altitude of $h_{park} = 200$ km and one of four reference inclinations as provided in Table 1. Then, a first Fregat burn will put the payload on an intermediate transfer orbit with apogee altitude equal to the final

orbit altitude and perigee altitude equal to 200 km. During this burn, the Fregat upper stage can also provide a small change of inclination as needed. Finally, after coasting up to apogee of the intermediate transfer orbit, a second Fregat burn raises the perigee and any remaining inclination change is carried out after which the spacecraft separates from the Fregat upper stage. This description suggests that the Soyuz Fregat upper stage approximates a two-body Hohmann transfer from a low Earth, 200 km circular parking orbit (hereafter simply referred to as 'parking orbit') to the final target orbit, where any inclination change is distributed over the first (apogee raise) Fregat burn, ΔV_1, and second (perigee raise) Fregat burn, ΔV_2, see also Fig. 3.

When applying this approach to launch a spacecraft into a general elliptical target orbit with inclination i_{target} and apogee and perigee altitudes h_{apo} and h_{peri}, the following Fregat burns are needed:

$$\Delta V_1 = \sqrt{\frac{\mu_E}{R_e + h_{park}}} \sqrt{2 + e_t - 2\sqrt{1 + e_t} \cos\left(f_{\Delta i}\Delta i\right)} \quad [6]$$

$$\Delta V_2 = \sqrt{\frac{\mu}{R_e + h_{apo}}} \cdot$$
$$\frac{}{\sqrt{2 - e_t - e_{target} - 2\sqrt{1 - e_t}\sqrt{1 - e_{target}} \cos\left((1 - f_{\Delta i})\Delta i\right)}} \quad [7]$$

where μ_E is the gravitational parameter of the Earth, $R_e = 6378$ km is the radius of the Earth and $f_{\Delta i}$ is the fraction of the total inclination change $\Delta i = i_{target} - i_{park}$ provided during the first burn, with $0 \le f_{\Delta i} \le 1$. Furthermore, the eccentricity of the intermediate transfer orbit, e_t, is given by:

$$e_t = \frac{h_{apo} - h_{park}}{2R_e + h_{apo} + h_{park}} \quad [8]$$

and the eccentricity of the target orbit, e_{target}, equals:

$$e_{target} = \frac{h_{apo} - h_{peri}}{2R_e + h_{apo} + h_{peri}} \quad [9]$$

Finally, using the rocket equation, the mass that can be injected into the target orbit (i.e. the spacecraft mass plus adapter/dispenser mass of 100 kg[15]) can be determined from:

$$m_{target} = m_{park} \exp\left[-\Delta V_{tot} / \left(I_{sp_F} g_0\right)\right] - m_{fregat} \quad [10]$$

with $\Delta V_{tot} = \Delta V_1 + \Delta V_2$, $I_{sp_F} = 330$ s the specific impulse of the Fregat upper stage[15], g_0 the Earth gravity constant (9.80665 m/s²), $m_{fregat} = 1000$ kg the mass of the Fregat upper stage[15] and m_{park} the maximum mass in the parking orbit. This mass includes the mass of the Fregat upper stage, the adapter and the

spacecraft and is obtained from extrapolating data in Ref. 15 and is presented in Table 2.

Parking orbit inclination, deg	Maximum mass (Fregat + adapter + spacecraft) in parking orbit, kg
51.8	7,285
64.9	6,449
70.4	6,294
95.4	6,275

Table 2 Soyuz launch vehicle performance in 200 km circular parking orbit

A validation of this approach is provided through the graphs in Fig. 4, which show the maximum mass (spacecraft + adapter) that can be launched into a circular (a) or elliptical (b) target orbit and the penalty on the launch performance when an inclination change needs to be performed (c). The lines indicate the performance as provided by Ref. 15, while the round markers indicate the performance according to the model in Eqs. [6] to [10]. Note that the best fit for Fig. 4c to the data in Ref. 15 was found for $f_{\Delta i} = 0.15$.

From the close resemblance between the two data sets in Fig. 4 it can be concluded that the launch model in Eqs. [6] to [10] is a good approximation of the Soyuz launch performance. It can therefore be applied in the design and optimisation of the pole-sitter transfer.

III.II   Transfer phase

As depicted in Fig. 3, the transfer phase starts from the target launch orbit up to insertion into the pole-sitter orbit. The initial condition therefore equals the Keplerian elements of the target orbit, while the final condition satisfies Eqs. [2] and [3].

While the launch phase is described using a two-body model, the transfer phase is modelled in the CR3BP using the equations of motion in Eq. [1]. Furthermore, the transfer can either be ballistic or be performed using low thrust, solar electric propulsion, causing the thrust-induced acceleration vector in Eq. [1] to become:

$$\mathbf{a} = \begin{cases} 0 & \text{Ballistic} \\ \dfrac{\mathbf{T}}{m} & \text{SEP} \end{cases} \quad [11]$$

with $\mathbf{T} = \begin{bmatrix} T_x & T_y & T_z \end{bmatrix}^T$ the SEP thrust vector in the reference frame of Fig. 1 and m the instantaneous mass of the spacecraft. To compute this mass, the equations of motion have to be augmented with the following equation to account for the mass consumption by the SEP thruster:

$$\dot{m} = -\frac{T}{I_{sp} g_0} \quad [12]$$
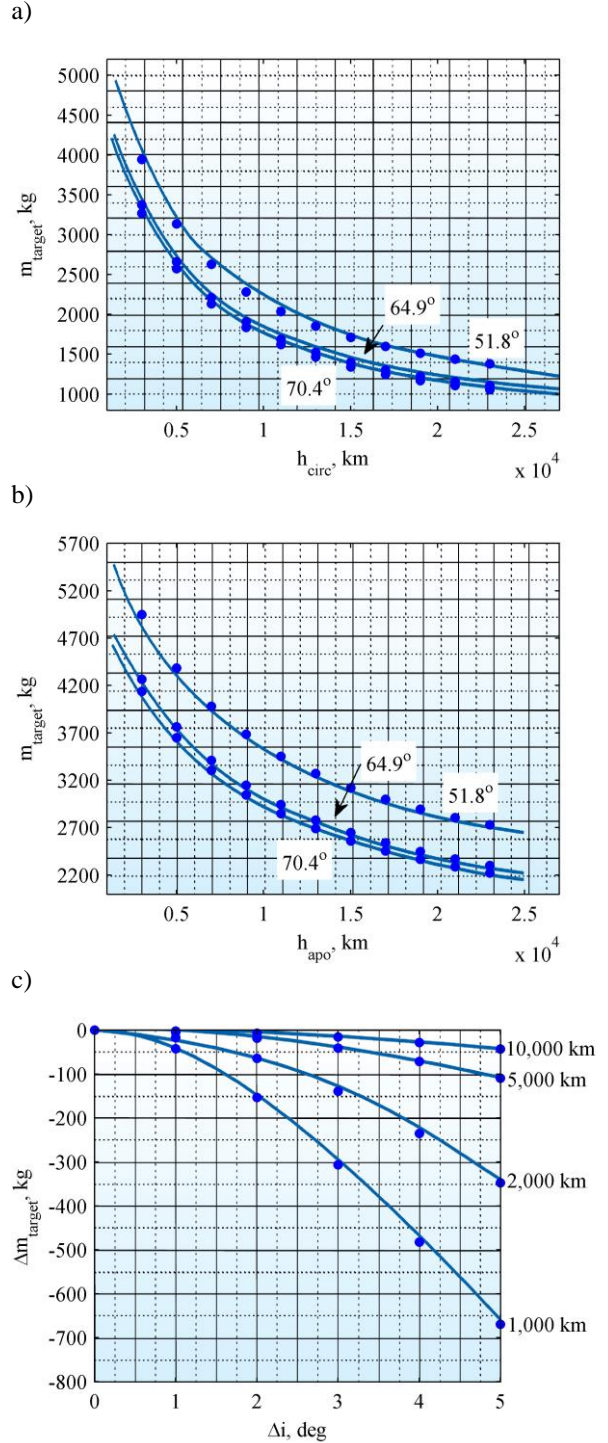
a)

b)

c)

Fig. 4 Comparison of launch vehicle performance (spacecraft + adapter mass) from model (round markers) and from Ref. 15 (solid lines) for circular orbits (a) and elliptical orbits with a perigee altitude of 200 km (b) for different inclinations of the initial parking orbit. (c) Penalty for an inclination change from a 51.8° orbit with different altitudes.

with $I_{sp} = 3200$ s the specific impulse of the SEP thruster (in correspondence with the SEP thruster used for the pole-sitter mission in Ref. 11).

IV. BALLISTIC TRANSFER PHASE

Ballistic trajectories to the pole-sitter orbit can be obtained by generating the manifolds that wind onto the pole-sitter orbit. Here, this is done through a simple backwards integration of the equations of motion in Eqs. [1] and [11] starting from the initial conditions in Eqs. [2] and [3] for different locations, θ, along the pole-sitter orbit. Note that no manoeuvre needs to be applied. When allowing a maximum integration time of a quarter of a year, truncating the manifold at the point of closest approach to the Earth and discarding those that attain an altitude of less than 200 km, the results in Fig. 5 are obtained.

The performance of the different manifolds can be assessed by linking the launch phase, as described in Section III.I, to the start of each ballistic transfer. For this, the initial state vector of the manifold is transformed from the CR3BP reference frame in Fig. 1 to an inertial, Earth fixed, equatorial reference frame and expressed in Keplerian elements. With the requirement that the mass at the end of the transfer phase should equal 1000 kg and the fact that the transfer phase is ballistic, the mass at the end of the launch phase, m_{target}, should also equal 1000 kg. Using Eqs. [6] to [10], the mass required to be launched into the parking orbit, m_{park}, can then be computed and is used as performance indicator.

To maximise this mass, rather than truncating the manifold at the point of closest approach, a simple optimisation can find the optimum location along the manifold to link the launch phase (i.e. the optimum time spend in the transfer phase, t_T) and the optimum initial condition of the integration, i.e. the point where the manifold winds onto the pole-sitter orbit, θ. A genetic algorithm[16] with suggested default settings and decision vector $\mathbf{x} = \begin{bmatrix} t_T & \theta \end{bmatrix}$ is used for this. Note that, in case the altitude along the manifold becomes less than 200 km or if the eccentricity of the initial state vector is larger than 1, a penalty is introduced on the objective function through a simple *if* statement. The latter constraint is introduced because the launch model in Section III.I can only consider non-escape launches. Finally, the optimisations are carried out five times to account for the randomness that is inherent in the genetic algorithm.

The best solutions found are provided in Fig. 6 and Table 3 for both the constant altitude and the variable altitude pole-sitter orbits and for each of the inclinations of the parking orbit. The results show that, the smaller the inclination of the parking orbit, the larger m_{park}.

This is due to the fact that the inclination of the initial state vector of the transfer phase is close to 90°. With the transfer phase being ballistic, the launcher has to provide the required change between the parking orbit inclination and the inclination of the transfer, which increases for decreasing inclination of the parking orbit and thus penalises the performance. However, for all inclinations, the results show that a ballistic transfer is feasible using a Soyuz launch, since the mass required in the parking orbit is smaller than the maximum Soyuz performance in Table 2.

Finally, comparing the results for the constant altitude pole-sitter orbit with those for the variable altitude orbit shows only small variations in m_{park}, but a substantial increase in the transfer time for the variable altitude orbits, because the point of insertion into the pole-sitter orbit lies much farther from Earth.

Parking orbit inclination, deg	m_{park}, kg	t_T, days	θ, deg
Constant altitude pole-sitter			
51.8	5,921	34	80.6
64.9	5,780	34	79.3
70.4	5,736	34	259.4
95.4	5,671	34	259.3
Variable altitude pole-sitter			
51.8	5,884	64	144.1
64.9	5,769	64	143.9
70.4	5,736	64	144.3
95.4	5,690	47	295.7

Table 3 Minimised mass in 200 km altitude circular parking orbit m_{park}, transfer phase time t_T and location of insertion into the pole-sitter orbit for constant and variable altitude pole-sitter orbits and for different parking orbit inclinations.

V. LOW-THRUST TRANSFER PHASE

In order to improve the performance of the ballistic pole-sitter transfer in terms of mass required in the parking orbit, this section investigates the use of low-thrust propulsion during the transfer phase. For this, the optimal control problem in the transfer phase needs to be solved, while linking the initial state vector of the transfer phase with the launch phase in the objective function. Hereafter some specific parts of this method are considered in detail.

V.I   Optimal control solver

To solve the optimal control problem, two different free and open source optimal control solvers are used to compare and validate the individual performances: GPOPS[17] coded in MATLAB® and PSOPT[18] coded in
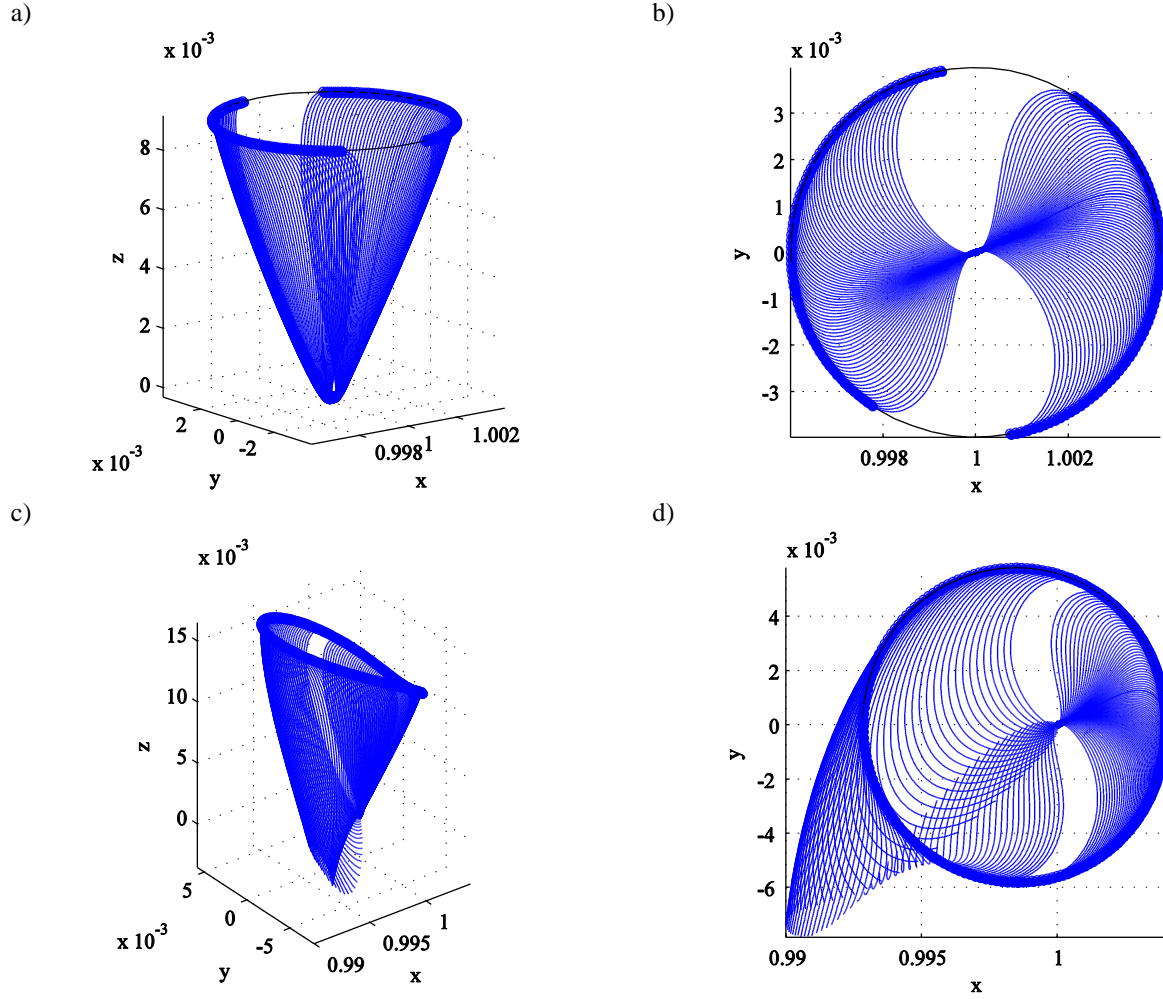
a)

b)

c)

d)

Fig. 5 Manifolds in CR3BP reference frame winding onto a constant altitude pole-sitter orbit (a, b) and a variable altitude pole-sitter orbit (c, d) where manifolds with a minimum altitude of less than 200 km are omitted.

a) $i_{park} = 51.8°$

b) $i_{park} = 69.4°$
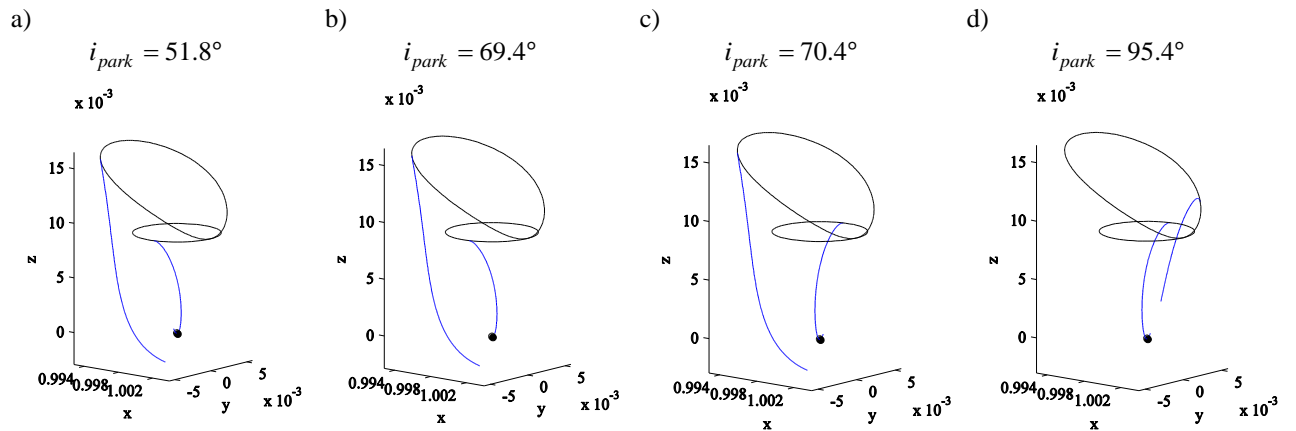
c) $i_{park} = 70.4°$

d) $i_{park} = 95.4°$

Fig. 6 Optimum ballistic pole-sitter transfer phases for constant and variable altitude pole-sitter orbits for different inclinations of the parking orbit.

C++. Both implement a direct pseudospectral method to solve the optimal control problem. The time interval is discretized into a finite number of collocation points and Legendre or Chebyshev polynomials are used to approximate and interpolate the time dependent variables at the collocation points. This way, the infinite dimensional optimal control problem is transformed into a finite dimension non-linear programming (NLP) problem. In case of GPOPS the NLP problem is solved using the software package SNOPT (Sequential Non-linear OPTimizer)[19], while PSOPT can make use of either SNOPT or IPOPT (Interior Point OPTimizer)[20].

V.II   States, controls and dynamics

For the pole-sitter transfer, the state vector is given by the Cartesian position and velocity vectors in the CR3BP reference frame of Fig. 1 and the mass of the spacecraft, while the controls are the Cartesian thrust components in the CR3BP. Note that the Cartesian thrust components are used rather than two thrust angles and the thrust magnitude as these may give rise to ambiguities[21].

Finally, the dynamics of the spacecraft in the SEP pole-sitter transfer are given by Eqs. [1], [11] and [12]. Also note that the new units introduced in Section II cause the magnitude of the dimensionless mass and thrust to be in the order of 10^{-18}. Therefore, to prevent problems with machine precision and the NLP tolerance, the mass and thrust magnitude are manually scaled back to their physical unites, and are adapted appropriately for use in the equations of motion.

V.III   Objective function

The objective function of the SEP pole-sitter transfer is equal to the objective function of the ballistic transfer:

$$J = -m_{park} \qquad [13]$$

For this, the start of the SEP transfer phase is linked to the launch phase by converting the initial state vector similarly to what was described in Section IV: from the CR3BP reference frame to an inertial, Earth fixed, equatorial reference frame. A further transformation to Keplerian elements enables the calculation of the mass in the parking orbit through Eqs. [6] to [10].

To be able to compute an objective function value even for escape orbits, an eccentricity at the start of the transfer phase of larger than 1 is transformed to a value less than 1 as illustrated in Fig. 7a. For this the following step function is used:

$$e_1 = H_1 \left(e_{step} - e_0 \right) + e_0 \qquad [14]$$

with e_0 the original eccentricity, e_1 the transformed eccentricity and H_1 a smooth Heaviside function defined as:

$$H_1 = \frac{1}{2} \left(1 + \tanh \left(\frac{e_0 - e_{step}}{a_{step}} \right) \right) \qquad [15]$$

with $e_{step} = 0.995$ and $a_{step} = 0.001$. Note that the smooth Heaviside function is used to prevent non-differentiable points in the objective function. Because the objective function value computed with the transformed eccentricity is not realistic it is penalised as follows, see Fig. 7b:

$$J = -f_{penalty} m_{park} \qquad [16]$$

with

$$f_{penalty} = H_1 \left(f_{step} - 1 \right) + 1 \qquad [17]$$

and $f_{step} = 0.001$.

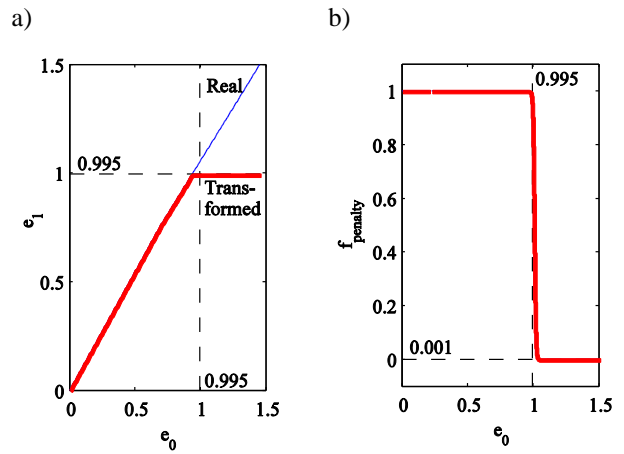a)   b)

Fig. 7 Transformed eccentricity (a) and corresponding penalty on objective function (b) to enable use of launch model for escape orbits.

V.IV   Constraints

Three different types of constraints can be distinguished for the SEP pole-sitter transfer, including bounds on the states, controls and time, event constraints and path constraints.

The most important bound is the one on the maximum thrust magnitude, which is set to $T_{max} = 0.25$ N so that it is large enough to enable the pole-sitter orbits presented in Ref. 11.

Considering the events, the state vector at the end of the SEP transfer should fully coincide with the pole-sitter orbit conditions. Furthermore, although the penalty on the objective function should already guide the final optimal solution to an eccentricity smaller than 1, an event is included to ensure this:

$$e_0 - e_{max} \leq 0 \qquad [18]$$

with e_0 the eccentricity at the start of the transfer phase and $e_{max} = 0.995$ the maximum allowable eccentricity.

A final event is included to prevent numerical problems with the automatic differentiation used by GPOPS and PSOPT. The numerical difficulties arise when the perigee of the target launch orbit coincides with the parking orbit. Then, the second Fregat burn, ΔV_2, becomes zero, its derivative infinite and the optimal control solver exits with an error. Therefore, the following constraint is taken into account to ensure that the perigee of the target launch orbit and the parking orbit do not coincide:

$$a_0(1-e_0) - r_{p,\min} \geq 0 \qquad [19]$$

with a_0 the semi-major axis at the start of the transfer phase and $r_{p,\min}$ the minimum required perigee radius, which is set to 6628 km, i.e. 50 km above the parking orbit.

Finally, because the Cartesian thrust components are used as control vector, a path constraint needs to be included to limit the total thrust magnitude to $T_{\max}$ along the whole trajectory.

V.V   Results
Using the results for the ballistic transfers in Section IV as initial guess, the results in Fig. 8, Fig. 9 and Table 4 are generated. Only the results obtained with PSOPT are included since GPOPS and PSOPT provided very similar results, both in terms of the mass required in the parking orbit, the transfer trajectories and the thrust profiles.

Comparing the results for the SEP transfers with the results of the ballistic transfer (which are included in Table 4 for comparison) shows a decrease in the mass required in the parking orbit of 24 kg to 232 kg. These mass savings can be attributed to the fact that, rather than the Fregat upper stage having to perform the inclination change between the parking orbit and the pole-sitter orbit (i.e. approximately 90°), the SEP
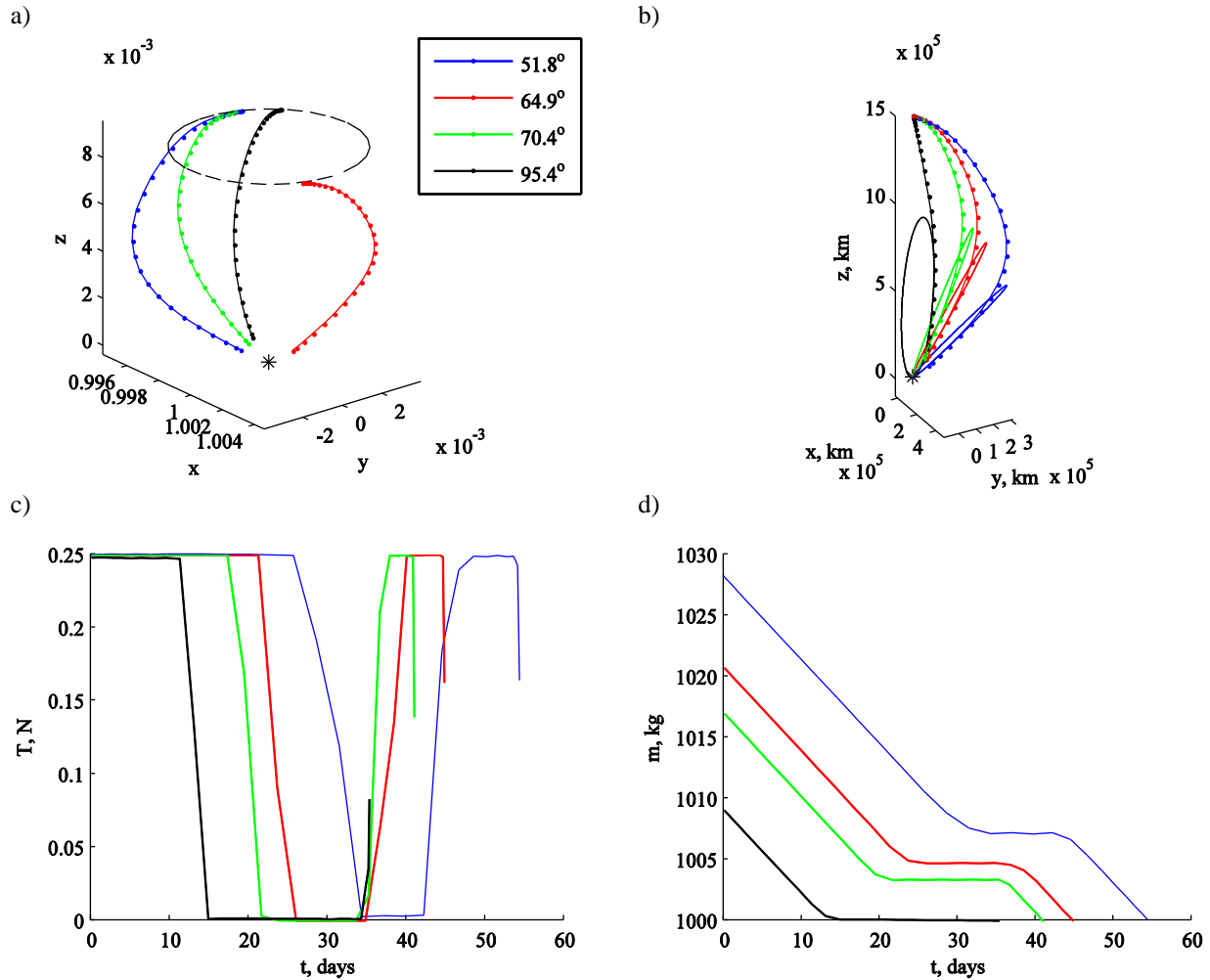

Fig. 8 Constant altitude pole-sitter: optimised SEP transfer phase in the CR3BP reference frame (a) and in an inertial, Earth fixed, equatorial reference frame (including the launch phase) (b), and the thrust (c) and mass (d) profiles for each value of the parking orbit inclination.
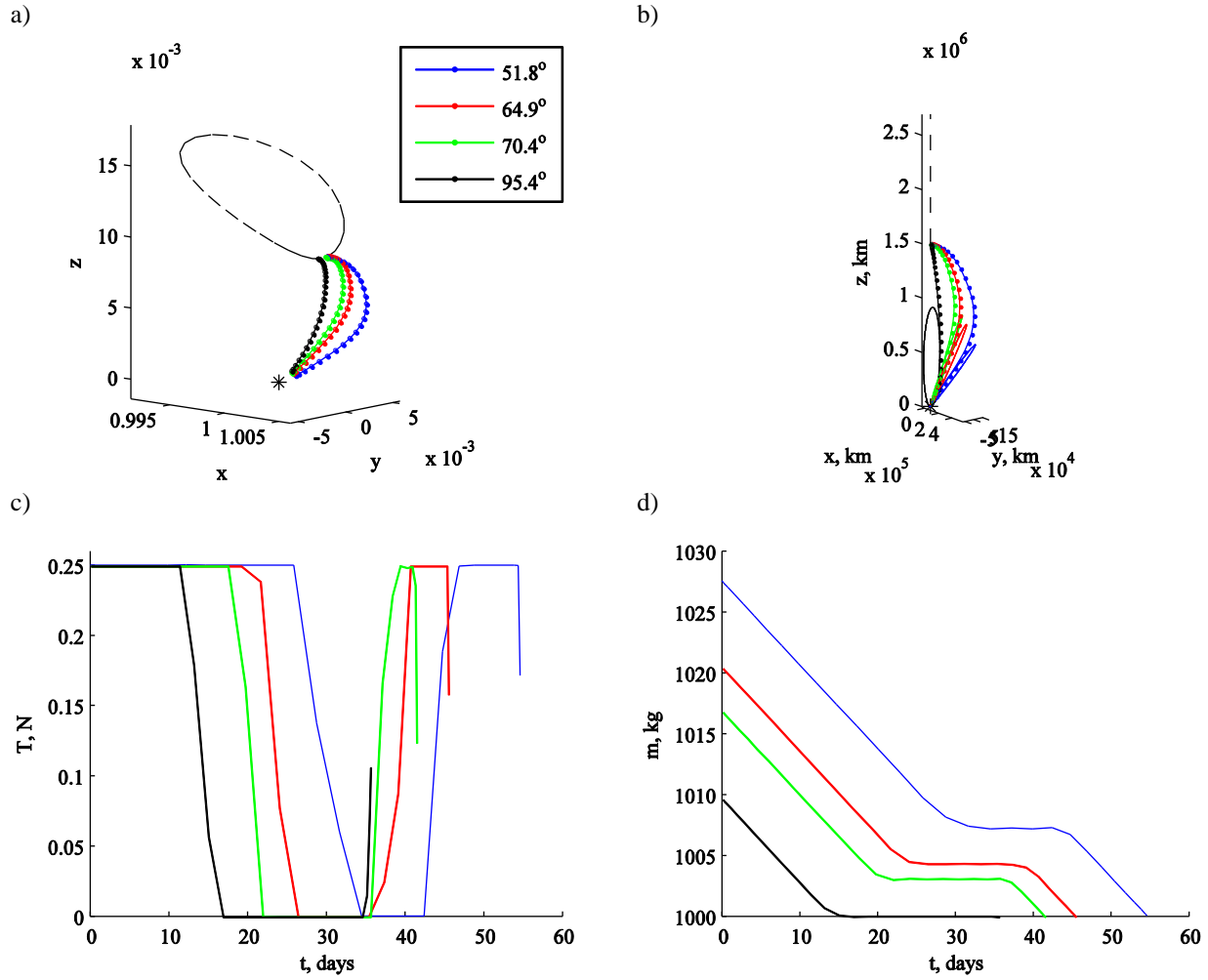
a)

b)

c)

d)

Fig. 9 Variable altitude pole-sitter: optimised SEP transfer phase in the CR3BP reference frame (a) and in an inertial, Earth fixed, equatorial reference frame (including the launch phase) (b), and the thrust (c) and mass (d) profiles for each value of the parking orbit inclination.

Parking orbit inclination, deg	Ballistic m_{park}, kg	SEP m_{park}, kg	Δm_{park}, kg	Time of flight, days	i_0, deg
Constant altitude pole-sitter					
51.8	5,921	5,689	232	55	52.0
64.9	5,780	5,673	107	45	65.1
70.4	5,736	5,665	71	41	70.7
95.4	5,671	5,647	24	36	95.2
Variable altitude pole-sitter					
51.8	5.884	5,691	193	54	51.9
64.9	5,769	5,674	95	45	65.1
70.4	5,736	5,666	70	41	70.7
95.4	5,690	5,647	43	35	95.3

Table 4 Constant altitude and variable altitude pole-sitters: comparison of minimised mass in 200 km altitude circular parking orbit m_{park} for the ballistic and SEP transfers, time of flight in transfer phase t_T and inclination at start of transfer phase i_0 for each value of the parking orbit inclination.

thruster can much more efficiently perform this inclination change. This is shown in Table 4, since the inclination at the start of the transfer phase, i_0, very closely matches the inclination of the parking orbit.

Finally, comparing the results for the constant and variable altitude pole-sitter orbits shows only very minor differences. That, in combination with the fact that the transfer phase for the variable altitude orbit always enters the pole-sitter around winter (see Fig. 9a), suggests that the performance of the transfer depends much more on the altitude of the pole-sitter orbit than on the time of year at which the spacecraft enters the pole-sitter orbit (as one might conclude from Fig. 8a). This leads to a very flexible launch window for the pole-sitter transfer.

VI. LOW-THRUST LAUNCH PHASE

In order to obtain a full low-thrust trajectory from low Earth orbit to the pole-sitter orbit, this section replaces the Fregat launch phase with a low-thrust spiral, see Fig. 10. The result will be a full low-thrust Earth to pole-sitter transfer.
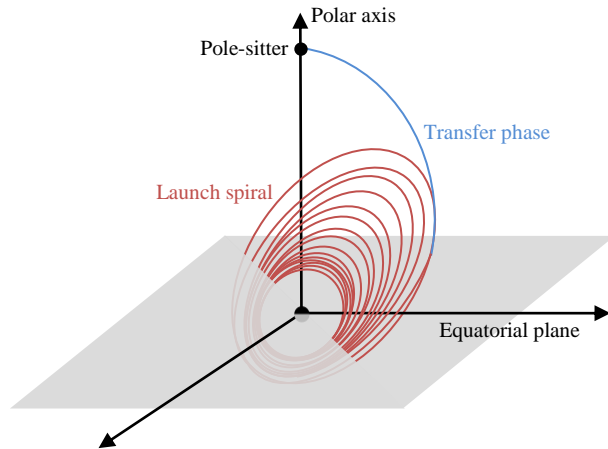

Fig. 10 Schematic of low-thrust launch spiral.

To model the low-thrust spiral, it is assumed that the transfer phase as provided in Fig. 8a and Fig. 9a remains unchanged. The problem then becomes to find the thrust profile in each revolution of the spiral such that the end of the spiral coincides with the start of the transfer phase. Furthermore, with the spiral expected to take many months, up to more than a year, the objective is to minimise the time spent in the spiral. Therefore, a locally optimal control profile, similarly to what has been suggested in Gao[14], is applied. This profile consists of the following three steering laws, which are illustrated in Fig. 11:

1) To change the semi-major axis, a tangential steering law is applied around perigee over an angle $2 p_s \pi$.
2) To change the eccentricity, a so-called inertial steering law is used where the spacecraft thrusts

perpendicular to the line of apsis around apogee over an angle $2 p_e \pi$.
3) To change the inclination, an out-of-plane steering law is applied around the nodal crossings over an angle $p_i \pi$, with opposite thrusting direction along the ascending and descending nodes.
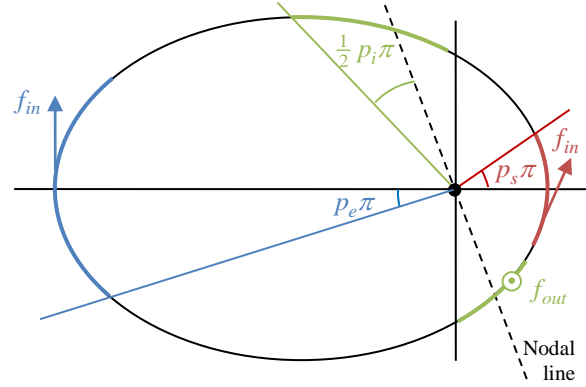

Fig. 11 Illustration of the launch spiral control profile.

The controls in the spiral thus include the thrust magnitudes of the in-plane, $f_{in} \geq 0$, and out-of-plane, $f_{out} \geq 0$, thrust accelerations and the parameters $-1 \leq p_s \leq 1$, $-1 \leq p_e \leq 1$ and $-1 \leq p_i \leq 1$ that represent the fraction of the orbit around perigee, apogee and the nodal line where one of three controls is applied. Note that positive and negative values for these three parameters indicate an increase and decrease in the corresponding orbital element, respectively.

To investigate the influence of different control profiles on the launch spiral through an integration of the full set of equations of motion would require a huge computational effort. Therefore, the orbital averaging technique is used, which approximates the equations of motion by calculating the change in the orbital elements after each revolution and dividing it by the orbital period. This change in the orbital elements can be computed when starting from Gauss' variational equations[22] in terms of eccentric anomaly, E:

$$\frac{da}{dE} = \frac{2a^3}{\mu_C}\left(f_r e \sin E + f_\theta \sqrt{1-e^2}\right)$$

$$\frac{de}{dE} = \frac{a^2}{\mu_C}\left[f_r\left(1-e^2\right)\sin E + f_\theta\left(2\cos E - e - e\cos^2 E\right)\sqrt{1-e^2}\right] \quad [20]$$

$$\frac{di}{dE} = \frac{a^2}{\mu_C}f_n\left(\frac{\cos\omega\cos E - e\cos\omega}{\sqrt{1-e^2}} - \sin\omega\sin E\right)\left(1-e\cos E\right)$$

$$\frac{d\Omega}{dE} = \frac{a^2}{\mu_C}f_n\left(\frac{\sin\omega\cos E - e\sin\omega}{\sqrt{1-e^2}} + \cos\omega\sin E\right)\frac{\left(1-e\cos E\right)}{\sin i}$$

$$\frac{d\omega}{dE} = -\cos i\frac{d\Omega}{dE} - \frac{a^2}{e\mu_C}\left[f_r\left(\cos E - e\right)\sqrt{1-e^2} - f_\theta\left(2-e^2 - e\cos E\right)\sin E\right]$$

with a, e, i, Ω and ω the standard Keplerian elements and μ_C the gravitational parameter of the central body. Note that Eq. [20] holds under the

assumption that the thrust acceleration is much smaller than the gravitational acceleration.

Depending on the steering law applied, the acceleration components in radial, f_r, transverse, f_θ, and normal, f_n, direction in Eq. [20] are given by:

$$f_r = \begin{cases} f_{in} e \sin E / \sqrt{1 - e^2 \cos^2 E} & \text{Tangential} \\ f_{in} \sin \theta & \text{Inertial} \\ 0 & \text{Out-of-plane} \end{cases} \quad [21]$$

$$f_\theta = \begin{cases} f_{in} \sqrt{1-e^2} / \sqrt{1 - e^2 \cos^2 E} & \text{Tangential} \\ f_{in} \cos \theta & \text{Inertial} \\ 0 & \text{Out-of-plane} \end{cases} \quad [22]$$

$$f_\theta = \begin{cases} 0 & \text{Tangential} \\ 0 & \text{Inertial} \\ f_{out} & \text{Out-of-plane} \end{cases} \quad [23]$$

with θ the true anomaly.

Substituting Eqs. [21] to [23] into Eq. [20] and integrating over the eccentric anomalies where the separate steering laws are applied, provides the change in orbital elements after one revolution. Note that during the integration the orbital elements are assumed to be constant. Subsequently dividing by the orbital period, P, gives the sought for approximation of the equations of motion. The full derivation has been performed by Gao[14] and only the result is repeated here:

$$\frac{da}{dt} = \frac{1}{P}\left(\frac{2a^3}{\mu_C} f_{in} \operatorname{sign}(p_s) \left[\sqrt{1-e^2} E + \left(1 - \sqrt{1-e^2}\right)(0.5E - 0.25\sin 2E) \right]_{E_{s,0}}^{E_{s,f}} + \frac{2a^3}{\mu_C} f_{in} \operatorname{sign}(p_e) \sqrt{1-e^2} \left[\sin E \right]_{E_{e,0}}^{E_{e,f}} \right)$$

$$\frac{de}{dt} = \frac{1}{P}\left(\frac{2a^2}{e\mu_C}(1-e^2) f_{in} \operatorname{sign}(p_s) \left(\frac{-e^2}{\sqrt{1-e^2}c} [0.5E + 0.25\sin 2E]_{E_{s,0}}^{E_{s,f}} + \left[\ln\left(\sin E + \frac{1}{e}\sqrt{1-e^2\cos^2 E} \right) \right]_{E_{s,0}}^{E_{s,f}} \right) \right)$$

$$+ \frac{1}{P}\left(\frac{a^2}{\mu_C} f_{in} \operatorname{sign}(p_e) \sqrt{1-e^2} [1.5E - 2e\sin E + 0.25\sin 2E]_{E_{e,0}}^{E_{e,f}} \right) \quad [24]$$

$$\frac{di}{dt} = \frac{1}{P}\frac{a^2}{\mu_C} f_{out} \operatorname{sign}(p_i) \sum_{i=1}^{2}\left[\frac{(1+e^2)\cos\omega\sin E - 1.5eE\cos\omega - 0.25e\cos\omega\sin 2E}{\sqrt{1-e^2}} + \sin\omega\cos E - 0.25e\sin\omega\cos 2E \right]_{E_{n_i,0}}^{E_{n_i,f}}$$

$$\frac{d\Omega}{dt} = \frac{1}{P}\frac{a^2}{\mu_C \sin i} f_{out} \operatorname{sign}(p_i) \sum_{i=1}^{2}\left[\frac{(1+e^2)\sin\omega\sin E - 1.5eE\sin\omega - 0.25e\sin\omega\sin 2E}{\sqrt{1-e^2}} - \cos\omega\cos E + 0.25e\cos\omega\cos 2E \right]_{E_{n_i,0}}^{E_{n_i,f}}$$

$$\frac{d\omega}{dt} = \frac{1}{P}\left(\frac{-2a^2}{e^2\mu_C}\sqrt{1-e^2} f_{in} \operatorname{sign}(p_s) \left[\sqrt{1-e^2\cos^2 E} + \sin^{-1}(e\cos E) \right]_{E_{s,0}}^{E_{s,f}} + \frac{-a^2}{e\mu} f_{in} \operatorname{sign}(p_e)[0.25\cos 2E - e\cos E]_{E_{e,0}}^{E_{e,f}} \right) - \cos i \frac{d\Omega}{dt}$$

The summation is included to account for the out-of-plane thrust arcs around both nodal crossings and the subscripts '0' and 'f' indicate the initial and final value of the eccentricities E_s, E_e and E_n during which the tangential, inertial and out-of-plane steering occur, respectively. Note that Eq. [24] includes the approximation of two elliptic integrals, which appeared to be accurate for $c = 0.8$[14]. Finally, the change in mass is given by:

$$\frac{dm}{dt} = -\frac{mf_{in}}{I_{sp}g_0}\frac{1}{n}\left(E_{s,f} - e\sin E_{s,f} - \left(E_{s,0} - e\sin E_{s,0} \right) \right.$$

$$\left. + E_{e,f} - e\sin E_{e,f} - \left(E_{e,0} - e\sin E_{e,0} \right) \right) \quad [25]$$

$$-\frac{mf_{out}}{I_{sp}g_0}\frac{1}{n}\sum_{i}^{2}\left(E_{n_i,f} - e\sin E_{n_i,f} - \left(E_{n_i,0} - e\sin E_{n_i,0} \right) \right)$$

which leads to a slightly conservative approach as the in-plane and out-of-plane thrust components are not combined into one single thrust component.

VI.I Optimal control problem

To find the optimum control profile in the spiral such that the boundary conditions are satisfied (i.e. the end of the spiral coincides with the start of the transfer phase) and the time of flight is minimised, the approach defined in the previous subsections is implemented in PSOPT. The state variables, $\mathbf{x}$, are the first five orbital elements in an inertial, Earth fixed equatorial reference frame and the spacecraft mass:

$$\mathbf{x} = \begin{bmatrix} a & e & i & \Omega & \omega & m \end{bmatrix} \quad [26]$$

The initial and final state vectors are given by the parking orbit and the initial state vector of the transfer phase, which is indicated by the subscript '$T,0$':

$$\mathbf{x}_0 = \begin{bmatrix} R_e + h_{park} & 0.01 & i_{park} & \Omega_{park} & \omega_{park} & m_{park} \end{bmatrix} \quad [27]$$

$$\mathbf{x}_f = \begin{bmatrix} a_{T,0} & e_{T,0} & i_{T,0} & \Omega_{T,0} & \omega_{T,0} & m_{T,0} \end{bmatrix} \quad [28]$$

with the ascending node, argument of perigee and mass in the parking orbit free. Note that the eccentricity of the parking orbit is increased from zero to 0.01 in order for the fifth equation in Eq. [24] to hold, as it approaches a singularity for $e = 0$[23].

The controls are the parameters indicating the size of the thrust arc for each steering law and the in-plane and out-of-plane thrust magnitudes:

$$\mathbf{u} = \begin{bmatrix} p_s & p_e & p_i & T_{in} & T_{out} \end{bmatrix} \quad [29]$$

The equations of motion are given by Eq. [24] and the following path constraints are included:

$$\left| p_s \right| + \left| p_e \right| \leq 1 \quad [30]$$

$$\sqrt{T_{in}^2 + T_{out}^2} \leq T_{max} \quad [31]$$

The first path constraint ensures that the thrust arcs for tangential and inertial steering do not overlap, while the second path constraint ensures that the total thrust magnitude does not exceed the maximum thrust magnitude of $T_{max} = 0.25$ N.

Finally, considering the fact that the inclination of the parking orbit is very close to the inclination at the start of the transfer, two dimensional initial guesses are used. They can easily be generated through a trial and error method until low-thrust spirals are obtained that closely match the boundary constraints.

VI.II   Results

Results for the low-thrust spiral are shown in Table 5 and detailed results are provided in Fig. 12 and Fig. 13 for the transfer to the constant altitude pole-sitter and for a parking orbit inclination of 95.4°. The results show a dramatic decrease in the mass required in the parking orbit when the low-thrust spiral, rather than the Fregat launch, is employed: on average 4373 kg. However, this comes at an equally dramatic increase in the time of flight. Considering a Hohmann transfer time for the Fregat launch results in launch phase times of approximately 36 days, which increases to an average of 471 days for the low-thrust spiral. The reason for this is the fact that over 1800 revolutions are made, most of them in low Earth orbit, until enough altitude is gained to make the required substantial changes to the orbital elements.

Reintegration of the results in Fig. 13 using the full set of equations of motion showed very good accuracy of the orbital averaging technique up to the last few revolutions, where both the semi-major axis

and eccentricity become very large and the assumptions made for the orbital averaging technique no longer hold (e.g. that the thrust acceleration is much smaller than the gravitational acceleration). The last few revolutions have therefore been reoptimised in order to match the result from PSOPT, using a sequential quadratic programming (SQP) method implemented in the MATLAB® function *fmincon*[24].

Parking orbit inclination, deg	m_{park}, kg	t_{sp}, days
Constant altitude pole-sitter		
51.8	1,308	470
64.9	1,301	467
70.4	1,295	469
95.4	1,285	473
Variable altitude pole-sitter		
51.8	1,308	472
64.9	1,298	475
70.4	1,294	472
95.4	1,287	469

Table 5 Low-thrust launch: minimised mass in 200 km altitude circular parking orbit, m_{park}, and time spent in spiral, t_{sp}, for constant and variable altitude pole-sitter orbits and for each value of the parking orbit inclination.
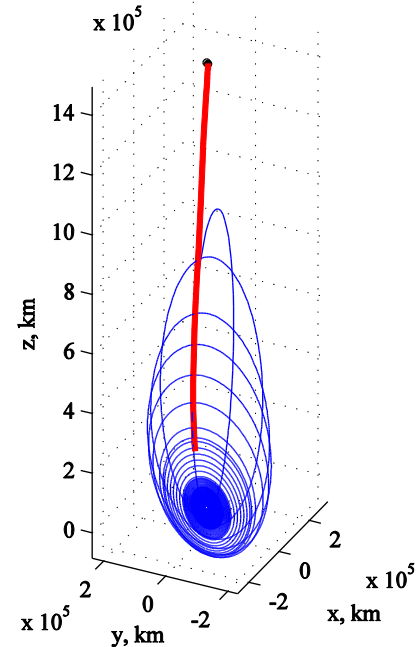

Fig. 12 Optimised launch spiral (in blue) and transfer phase (in red) to the constant altitude pole-sitter and for a parking orbit inclination of 95.4°.
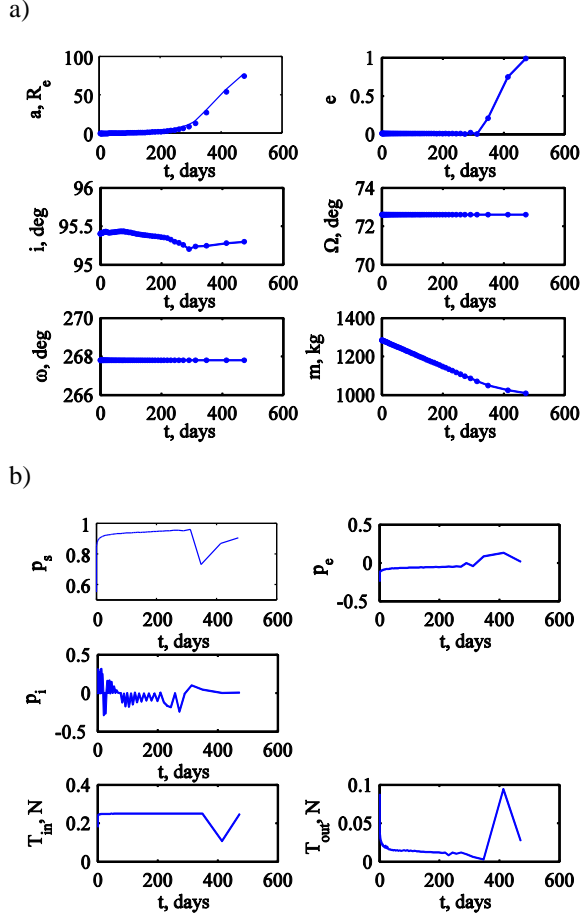
a)

b)

Fig. 13 State (a) and control (b) profile in low-thrust spiral for a transfer to the constant altitude pole-sitter and for a parking orbit inclination of 95.4°.

For this, the size of the different thrust arcs (given by the absolute value of the controls p_s, p_e and p_i) is kept unchanged and only the magnitude of the in-plane and out-of-plane thrust vectors are incorporated as design variables.

Bounds on the thrust magnitude of 0.25 N (as used in Section VI.I) are imposed, i.e. -0.25 N $\leq T \leq$ 0.25 N, where the sign takes over the function of the sign of the controls p_s, p_e and p_i in order to increase/decrease the orbital elements.

The results are provided in Fig. 14 for the transfer to the constant altitude pole-sitter orbit and for a parking orbit inclination of 51.8°. It provides both the solution from PSOPT and the original and reoptimised integrated solutions, and shows that, within a maximum thrust magnitude of 0.25 N, the reoptimised result closely matches the result from PSOPT.

Finally, note that the results in this section exclude any perturbation on the low-thrust spiral. However, it can be expected that the J_2 effect and shadowing have a significant influence on the spiral at low altitudes, while third body perturbations from the Sun will have a considerable effect at larger altitudes. These perturbations will be considered in future analyses.
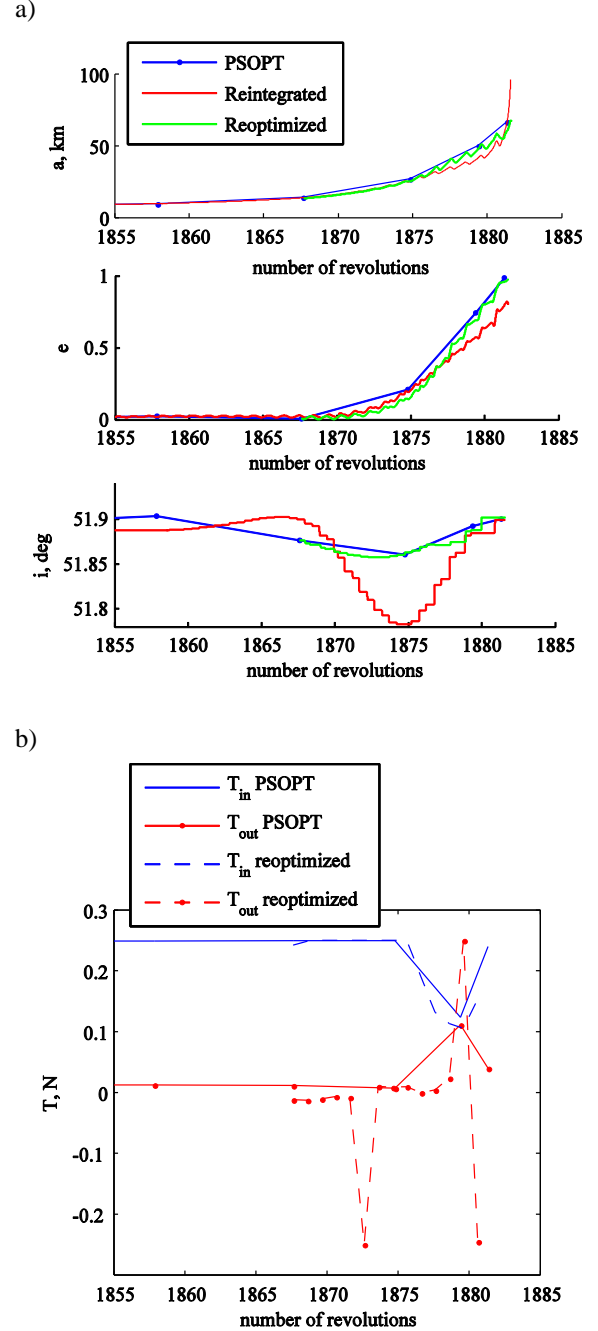
a)

b)

Fig. 14 Reoptimised integrated solution to match the result from PSOPT for the transfer to the constant altitude pole-sitter orbit and for a parking orbit inclination of 51.8°. a) States. b) In-plane and out-of-plane thrust components.

VII. CONCLUSIONS

In this paper, the feasibility of transfers from a low Earth parking orbit to a pole-sitter position has been investigated. Both ballistic and low-thrust SEP transfers have been considered as well as transfers to constant altitude (0.01 AU) and variable altitude (0.01-0.018 AU) pole-sitter orbits. By distinguishing between a launch phase and a transfer phase, the trajectory could be modelled and optimised. The launch phase starts from the parking orbit up to a two-body, highly elliptic orbit that coincides with the start of the transfer phase. The launch phase has been investigated for both a launch using the Soyuz Fregat upper stage and for the use of a low-thrust SEP spiral. For the first option, a Hohmann transfer-like model has been developed, which was shown to closely match the performance in the launcher's manual. For the case of the low-thrust spiral, three locally optimal control laws were applied to the revolutions of the spiral and orbital averaging was used to significantly speed up the integration of the equations of motion. The transfer phase, which stretches from the end of the launch phase up to the pole-sitter orbit, has been modelled in the circular restricted three body problem and both ballistic and low-thrust SEP approaches have been considered. The full transfer has been optimised for the mass required in the low Earth parking orbit for a 1000 kg spacecraft to be inserted into the pole-sitter orbit.

When using a Fregat launch phase, masses of 5671 to 5921 kg and 5647 to 5691 kg are required in the parking orbit for the ballistic and SEP cases, respectively. The range in masses is introduced by considering different inclinations for the parking orbit, where the smallest mass is obtained for the inclination closest to 90° (i.e. the pole-sitter position). Mass savings of 24 kg to 232 kg can be achieved by using an SEP instead of a ballistic transfer phase. However, both cases are feasible as the mass required in the parking orbit is less than the maximum launcher performance. Comparing the performances for the constant and variable altitude pole-sitter orbits showed only minor differences. With the transfer phase for the variable altitude orbit always entering the pole-sitter at winter (i.e. at the closest distance to Earth), it could be concluded that the altitude of the pole-sitter orbit has a greater influence on the performance than the time of year at which the spacecraft is injected into the pole-sitter orbit, leading to a flexible launch window for the pole-sitter transfer. Finally, assuming the transfer phase fixed, the Fregat launch was replaced by the low-thrust SEP spiral. This allowed for another dramatic decrease in the mass required in the parking orbit, but at the cost of an increased time of flight: the mass was reduced to 1285 to 1308 kg, while the duration of the launch phase was increased from 36 to 471 days.

VIII. ACKNOWLEDGEMENTS

IX. REFERENCES

[1] P. Anderson, M. Macdonald, "Extension of Earth Orbits Using Low-Thrust Propulsion", in *21st AAS/AIAA Space Flight Mechanics Meeting*, New Orleans, 2011.

[2] J. Driver, "Analysis of an Acrtic Polesitter", *Journal of Spacecraft and Rockets*, vol. 17, n. 3, p. 263-269, 1980. DOI: 10.2514/3.57736

[3] M. A. Lazzara, A. Coletti, B. L. Diedrich, "The possibilities of polar meteorology, environmental remote sensing, communications and space weather applications from Artificial Lagrange Orbit", *Advances in Space Research*, 2011, In Press, Accepted Manuscript. DOI: 10.1016/j.asr.2011.04.026

[4] C. R. McInnes, "Dynamics, Stability, and Control of Displaced Non-Keplerian Orbits", *Journal of Guidance, Control, and Dynamics*, vol. 21, n. 5, p. 799-805, 1998. DOI: 10.2514/2.4309

[5] R. J. McKay, M. Macdonald, J. Biggs, C. McInnes, "Highly Non-Keplerian Orbits With Low-Thrust Propulsion", *Journal of Guidance, Control, and Dynamics*, vol. 34, n. 3, 2011.

[6] C. R. McInnes, "The Existence And Stability Of Families Of Displaced Two-Body Orbits", *Celestial Mechanics and Dynamical Astronomy*, vol. 67, p. 167-180, 1997. DOI: 10.1023/A:1008280609889

[7] J. Heiligers, M. Ceriotti, C. R. McInnes, J. D. Biggs, "Displaced Geostationary Orbit Design Using Hybrid Sail Propulsion", *Journal of Guidance, Control, and Dynamics*, 2011, In Press, Accepted Manuscript.

[8] J. Simo, C. R. McInnes, "Solar Sail Orbits at the Earth-Moon Libration Points", *Communications in Nonlinear Science and Numerical Simulation*, vol. 14, n. 12, p. 4191-4196, 2009. DOI: 10.1016/j.cnsns.2009.03.032

[9] D. J. Grebow, M. T. Ozimek, K. C. Howell, "Advanced Modeling of Optimal Low-Thrust Lunar Pole-Sitter Trajectories", *Acta Astronautica*, vol. 67, p. 991-1001, 2010. DOI: 10.1016/j.actaastro.2010.04.024

[10] R. L. Forward, "Statite: A spacecraft that does not orbit", *Journal of Spacecraft and Rockets*, vol. 28, n. 5, p. 606-611, 1991. DOI: 10.2514/3.26287

[11] M. Ceriotti, C. R. McInnes, "Generation of Optimal Trajectories for Earth Hybrid Pole Sitters", *Journal of Guidance, Control, and Dynamics*, vol. 34, n. 3, p. 847-859, 2011. DOI: 10.2514/1.50935

[12] O. M. Golan, J. V. Breakwell, "Low Thrust Power-Limited Transfer For A Pole Squatter", in *AIAA/AAS Astrodynamics Conference*. American Institute of Aeronautics and Astronautics, Minneapolis, USA. p. 717-722, 1988.

[13] C. A. Kluever, S. R. Oleson, "Direct Approach for Computing Near-Optimal Low-Thrust Earth-Orbits Transfers", *Journal of Spacecraft and Rockets*, vol. 35, n. 4, p. 509-515, 1998.

[14] Y. Gao, "Near-Optimal Very Low-Thrust Earth-Orbit Transfers and Guidance Schemes", *Journal of Guidance, Control, and Dynamics*, vol. 30, n. 2, p. 529-539, 2007. DOI: 10.2514/1.24836

[15] Starsem, "The Soyuz Company", "Soyuz User's Manual (ST-GTD-SUM-01 - issue 3 - revision 0)", 2001.

[16] A. J. Chipperfield, P. J. Fleming, "The MATLAB Genetic Algorithm Toolbox", in *Proceedings of IEE Colloquium Applied Control Techniques Using MATLAB*, 1995.

[17] A. V. Rao, D. A. Benson, C. L. Darby, M. A. Patterson, C. Francolin, et al., "Algorithm 902: GPOPS, A MATLAB Software for Solving Multiple-Phase Optimal Control Problems Using The Gauss Pseudospectral Method", *ACM Transactions on Mathematical Software*, vol. 37, n. 2, p. 1-39, 2010. DOI: 10.1145/1731022.1731032

[18] V. M. Becerra, "Solving complex optimal control problems at no cost with PSOPT", in *Proceedings of IEEE Multi-conference on Systems and Control*, Yokohama, Japan, 2010.

[19] P. E. Gill, W. Murray, M. A. Saunders, "SNOPT: An SQP Alghorithm for Large-Scale Constrained Optimization", *SIAM J. Optim.*, vol. 12, n. 4, p. 979-1006, 2002.

[20] A. Wächter, L. T. Biegler, "On the implementation of an interior-point filter line-search algorithm for large-scale nonlinear programming", *Mathematical Programming*, vol. 106, n. 1, p. 25-57, 2006. DOI: 10.1007/s10107-004-0559-y

[21] J. T. Betts, "Practical Methods for Optimal Control Using Nonlinear Programming", Society for Industrial and Applied Mathematics (SIAM), Philadelphia, USA, 2001, pp. 150.

[22] R. H. Battin, "An Introduction to the Mathematics and Methods of Astrodynamics, Revised Edition", *AIAA Eduction Series*, ed. J.S. Przemieniecki, American Institute of Aeronautics and Astronautics, Inc., Reston, USA, 1999.

[23] J. A. Kechichian, "Orbit Raising with Low-Thrust Tangential Acceleration in Presence of Earth Shadow", *Journal of Spacecraft and Rockets*, vol. 35, n. 4, p. 516-525, 1998. DOI: 10.2514/2.3361

[24] M. Powell, "A fast algorithm for nonlinearly constrained optimization calculations", *Numerical Analysis*, ed. G. Watson, Springer Berlin / Heidelberg, 1978. DOI: 10.1007/BFb0067703